J. Fluid Mech. (1996), *vol.* 316, *pp.* 53–72

Thermoacoustic and buoyancy-driven transport in a square side-heated cavity filled with a near-critical fluid

By BERNARD ZAPPOLI[1], SAKIR AMIROUDINE[2], PIERRE CARLES[3] AND JALIL OUAZZANI[4]

[1] CNES, 18 Av. Edouard Belin, 31055 Toulouse Cedex, France

[2] Institut de Mécanique des Fluides, 1 rue Honnorat 13003 Marseille, France

[3] Institut National Polytechnique de Toulouse, Place des Hauts Murats, 31006 Toulouse, France

[4] ArcoFluid, IMT, Technopôle de Château Gombert, 13451 Marseille, France

(Received 22 March 1995 and in revised form 28 December 1995)

The mechanisms of heat and mass transport in a side-heated square cavity filled with a near-critical fluid are explored, with special emphasis on the interplay between buoyancy-driven convection and the Piston Effect. The Navier–Stokes equations for a near-critical van der Waals gas are solved numerically by means of an acoustically filtered, finite-volume method. The results have revealed some striking behaviour compared with that obtained for normally compressible gases: (i) heat equilibration is still achieved rapidly, as under zero-g conditions, by the Piston Effect before convection has time to enhance heat transport; (ii) mass equilibration is achieved on a much longer time scale by quasi-isothermal buoyant convection; (iii) due to the very high compressibility, a stagnation-point effect similar to that encountered in high-speed flows provokes an overheating of the upper wall; and (iv) a significant difference to the convective single-roll pattern generated under the same conditions in normal CO_2 is found, in the form of a double-roll convective structure.

1. Introduction

Heat transport in dense fluids is achieved by the basic mechanisms of convection, diffusion and radiation. However, in the case of low-heat-diffusing, near-critical fluids under zero-g conditions, it has been shown recently that a fourth mechanism of heat transport named the Piston Effect (PE) is responsible for very fast heat transport. This effect has been extensively studied and described in a number of papers, involving one-dimensional analytical (Zappoli 1992; Zappoli & Carles 1995) and numerical (Zappoli *et al.* 1990; Zappoli & Durand-Daubin 1994; Amiroudine *et al.* 1996) analyses, thermodynamical theory (Onuki, Hao & Ferrell 1990; Onuki & Ferrell 1990) and space-borne experiments (Guenoun *et al.* 1993; Bonetti *et al.* 1994; Straub 1965; Straub & Nitsche 1991, 1993) in low-gravity conditions where buoyant convection is strongly decreased. The PE mechanism originates from the particular properties of near-critical fluids, and more specifically from their diverging isothermal compressibility and vanishing thermal diffusivity. It can be briefly described by the following steps: (i) when a confined, near-critical fluid is heated from the boundaries, a thin thermal boundary layer forms; (ii) the fluid in this layer expands strongly due to the large compressibility, and induces an adiabatic compression of the bulk fluid; (iii) temperature is homogenized very rapidly, as a result of the adiabatic compression.

The thermoacoustic nature of this effect is now well established as well as its limits since it has been shown that all the heat brought to the wall of a container filled with a near-critical pure fluid could ultimately be transferred to the bulk at the speed of sound when approaching the critical point (Zappoli & Carles 1996; Amiroudine *et al.* 1996).

In connection with the heat-transport problem, the question which currently arises is whether this effect is still efficient under normal Earth gravity conditions or, in other words, if the fast heat transport observed on ground is due to the PE or to the very strong buoyant convection provoked by the high isothermal compressibility of near-critical fluids. However, beyond this question is the general problem of the description of convection, and more generally, of convective instabilities in hyper-compressible low-heat-diffusing dense fluids such as those encountered in near-critical conditions. Very little is known about the hydrodynamic behaviour of such systems. As a matter of fact, the hydrodynamics of critical fluids have not been developed by the critical-point community of physicists, and even the simpler situation of normally compressible non-Boussinesq fluids (such as perfect gases) has not been extensively studied from the hydrodynamic point of view. For example, Spradley & Churchill (1975) have studied pressure-driven (or thermoacoustic) motion which is generated by the local expansion of normally compressible fluid layers. They have shown that the thermally induced motion generated under microgravity conditions creates heat transport and thus enhances the global unsteady rate of heat transport, which remains of the same order of magnitude as diffusion. Paolucci (1982) has studied convection in strongly differentially heated cavities filled with a normally compressible non-Boussinesq gas using an acoustic filtering procedure. In addition to these studies of normally compressible media, in the early 1970s, a number of technical studies were devoted to the hydrodynamic behaviour of very compressible cryogenic supercritical oxygen, hydrogen or helium, which are known to be of a great technological interest. For example, Heinmiller (1970) has numerically studied convective flows in cryogenic oxygen tanks to obtain a description of the pressure collapse which follows a fast mechanical destratification of a near-critical fluid stored under microgravity. However, because of the inadequacy of computational resources available at that time, it was not possible to identify the basic heat-transport mechanisms even though some early published papers contained interesting features strongly linked with the current findings.

It is within the framework of the competition between thermoacoustic and buoyant convection that the problem of convection in hyper-compressible fluids is again of interest. Although no numerical solutions have been obtained with a reliable Navier–Stokes code written for a hyper-compressible near-critical fluid, some theoretical work has been done in an attempt to obtain stability criteria for fluid layers subjected to adverse temperature gradients (Gitterman & Steinberg 1970, 1971). More recently, a one-dimensional numerical description of a hydrodynamically stable cooled-from-below infinite layer (Boukari, Pego & Gammon 1995) has been given and the one-dimensional heat transport has also been studied under stable conditions (Zhong & Meyer 1995). Rather than examining the problem of a layer heated from below (with the unknown potential for Rayleigh–Bénard instability), we choose to look at the simpler case of convection (driven by both buoyancy and thermoacoustic effects) in a box which is heated from the side. It is demonstrated that the bulk of the temperature equilibration in this situation is achieved by the PE and not by buoyant convection. It has also been found that, due to the very high compressibility, significant density gradients remain even after the thermal field has been nearly completely homogenized by the PE, leading to a quasi-isothermal convective motion in a pure fluid

which is then responsible for mass equilibration. In addition, a stagnation-point overheating effect has been observed, although the flow velocity is very low. The next Section presents the model and governing equations, §3 describes the numerical method, and results are discussed in §4.

2. The model and governing equations

2.1. *The model*

As mentioned in the introduction, the main goal of this work is to investigate the competition between convective and thermoacoustic (PE) heat transport. We consider a square, two-dimensional cavity with a single, vertical, heated wall (on the left-hand side), the others being perfectly insulated (see figure 1). Under such conditions, the PE and buoyant convection both originate at the heated boundary while the other boundaries are not thermally active. This would not have been the case if one had considered, as in Zappoli & Carles (1995), an isothermal right-hand boundary which would have also led to a PE, but also, to a more complex situation without providing more information regarding the problem under study. The fluid is initially at rest and stratified in thermodynamic equilibrium such that

$$\frac{T'_0 - T'_c}{T'_c} = \mu \ll 1,$$

where T'_0 and T'_c are the initial and critical temperatures, respectively, and primes denote dimensional variables; μ defines the proximity to the critical point.

For the equation of state, we have chosen to use the van der Waals equation, although it is well known that it does not correctly describe the critical coordinates, namely it leads neither to the correct critical pressure nor to the correct critical exponents (i.e. the exponents describing the critical divergence of transport properties). Within the framework of the present work, however, this is not important since the pressure is involved in the equations only through its gradient, which is independent of the basic background pressure. Moreover, the use of this equation is consistent with earlier analytical results, and thus will allow comparison between them and the present findings. If necessary, when close to the critical point or for comparisons with experimental results, it is possible to use the restricted cubic model of Moldover *et al.* (1979) as the equation of state, although this has not been done in the present work. The transport equations have been chosen to be those of a viscous Newtonian heat-conductive fluid since the critical point is never approached so close as to render the Navier–Stokes equations invalid (Stanley 1971; Carles 1995). The van der Waals equation of state implicitly takes into account the divergence of the compressibility and of the heat capacity at constant pressure. In order to simulate the divergence of the thermal conductivity, a phenomenologic law has been introduced, in which the density dependence is not taken into account since departures from the critical density never exceed a fraction of a percent. If needed, more complete descriptions for heat conduction and/or heat capacities at constant pressure are available (Swinney & Henry 1973).

The following transport coefficients are considered:

$$\lambda = \frac{\lambda'}{\lambda'_0} = 1 + A\left(\frac{T' - T'_c}{T'_c}\right)^{-0.5}, \quad C_v = \frac{C'_v}{C'_{v0}} = 1, \quad \tilde{\mu} = \frac{\mu'}{\mu'_0} = 1,$$

where λ', C'_v and μ' are the thermal conductivity (in which $A = 0.75$), the heat capacity at constant volume and the viscosity, respectively; the subscript 0 represents the value

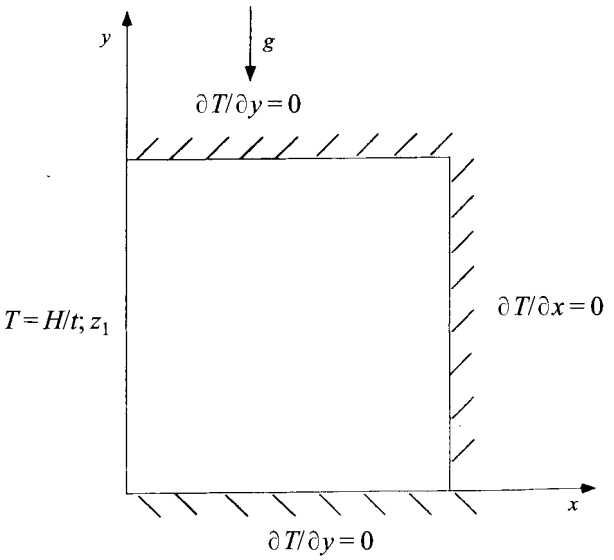

FIGURE 1. The two-dimensional model.

far from the critical point. The heat capacity at constant volume and the viscosity have been considered as constant and equal to the value for the perfect gas CO_2.

2.2. *The governing equations*

As just mentioned, the governing equations are those of a Newtonian viscous heat-conducting van der Waals gas initially at rest and stratified, subjected to a boundary heating. One should note that since the initial temperature is rather far from the critical one (1 K), we face a small initial stratification. The problem of strong stratification encountered when closer to the critical temperature might be quite different.

If the pressure is normalized with respect to the value it would have at the critical condition if the fluid were a perfect gas, and if the other variables are referred to their critical values, the governing equations can be written as follows:

continuity
$$\frac{\partial \rho}{\partial t} + \nabla \cdot (\rho \boldsymbol{v}) = 0, \tag{1}$$

momentum
$$\frac{\partial (\rho \boldsymbol{v})}{\partial t} + \nabla \cdot (\rho \boldsymbol{v}\boldsymbol{v}) = -\gamma^{-1} \nabla P + \epsilon [\nabla^2 \boldsymbol{v} + \tfrac{1}{3} \nabla (\nabla \cdot \boldsymbol{v})] + \frac{1}{F_r} \rho \boldsymbol{g}, \tag{2}$$

energy
$$\frac{\partial (\rho T)}{\partial t} + \nabla \cdot (\rho \boldsymbol{v} T) = -(\gamma - 1)(P + a\rho^2)(\nabla \cdot \boldsymbol{v}) + \frac{\epsilon \gamma}{P_r} \nabla \cdot [\{1 + A(T-1)^{-0.5}\} \nabla T]$$
$$+ \epsilon \gamma (\gamma - 1) \{v_{i,j} v_{j,i} + v_{i,j} v_{i,j} - \tfrac{2}{3} v_{i,i} v_{j,j}\}, \tag{3}$$

van der Waals equation of state
$$P = \frac{\rho T}{1 - b\rho} - a\rho^2. \tag{4}$$

The values of a and b in (4) ($a = 9/8$, $b = 1/3$) come from expressing the critical

coordinates as a function of a' and b' for the dimensional van der Waals equation, namely

$$T'_c = \frac{8a'}{27b'}, \quad \rho'_c = \frac{1}{3b'}, \quad P'_c = \frac{a'}{27b'^2},$$

in which $T'_c = 304.13$ K and $\rho'_c = 467.8$ kg m^{-3}.

The following non-dimensional variables have been defined:

$$\rho = \frac{\rho'}{\rho'_c}, \quad T = \frac{T'}{T'_c}, \quad P = \frac{P'}{\rho'_c R' T'_c}, \quad u = \frac{u'}{c'_0}, \quad v = \frac{v'}{c'_0}, \quad t = \frac{t' c'_0}{L'},$$

where $c'_0 = (\gamma R' T'_c)^{1/2}$ is the sound velocity for the perfect gas in which γ is the ratio of specific heats and $R' = 188.8$ J kg^{-1} K^{-1} is the perfect gas constant.

One should note that the energy equation (3) embodies strong variations of the heat conduction coefficient and as shown by this equation, it goes to infinity as $\mu^{-1/2}$ when T' approaches T'_c.

In (1)–(3), ϵ is a small parameter defined by $\epsilon = P_r t'_a / t'_d$ where $\epsilon = 2.6 \times 10^{-8}$, t'_d is the characteristic time of heat diffusion for the ideal gas, i.e.

$$t'_c = L'^2 / \kappa'_0,$$

κ'_0 is the thermal diffusivity of the ideal gas at critical density and t'_a is the characteristic acoustic time

$$t'_a = \frac{L'}{(\gamma R' T'_c)^{1/2}}.$$

In the case of CO_2 confined in a square cavity of side length of 10 mm, $t'_a = 35$ ms and $t'_d = 3 \times 10^3$ s. It must be noted that t'_d is not the characteristic time for diffusion in a supercritical fluid. Taking into account the vanishing thermal diffusivity of near-critical fluids, this characteristic time would be of order $t'_d / \mu^{1/2}$, which is even longer (Zappoli 1992).

The quantity $P_r = \nu'_0 / \kappa'_0$ is the Prandtl number (ν'_0 is the kinematic viscosity) and $F_r = c'_0 / L' g'_0$ is the acoustic Froude number ($g'_0 = 9.8$ m s^{-2} is Earth's gravity) where $P_r = 2.27$ and $F_r = 2.9 \times 10^3$.

Since the problem is to investigate the interaction between the PE and buoyant convection following a boundary heating, the characteristic time scale to be chosen to this end should be the shorter of the two, in order not to miss important possible interactions between them. The PE time scale defined by Zappoli (1992) is

$$\tau = \frac{\epsilon f(\mu, A)}{\mu^2} t,$$

with

$$f(\mu, A) = \mu \left(\frac{1}{A} + \frac{1}{\mu^{1/2}} \right).$$

The dimensional PE time scale is of the order of tenths for CO_2 a few K from T_c, but much shorter as one gets nearer. The convective time scale (the characteristic time for convection to start), which depends on the kinematic viscosity, is also of the order of a tenth of a second. The PE time scale is thus taken as its characteristic time while velocity is normalized with respect to the characteristic velocity on that time scale, i.e.

$$\boldsymbol{v}_\tau = \frac{\mu^2}{\epsilon f(\mu, A)} \boldsymbol{v}.$$

The dimensionless initial conditions can be written as

$$\rho_0(y) = 2 - e^{K(y-1)}, \quad T_0 = 1 + \mu, \quad P_0(y) = P_{01} + \tfrac{9}{4}\mu[1 - e^{K(y-1)}], \quad u = v = 0,$$

where $K = 4g\gamma/(9\mu F_r)$ and $P_{01} = \frac{3}{2}(1+\mu) - \frac{9}{8}$. The boundary conditions for the problem defined in the previous section are

$$u = v = 0 \quad \text{at all walls},$$

$$T(0, y, t) = H(t; \tau_1),$$

$$\frac{\partial T}{\partial x}(1, y, t) = \frac{\partial T}{\partial y}(x, 0, t) = \frac{\partial T}{\partial y}(x, 1, t) = 0.$$

The parameter τ_1 is the boundary-heating time scale which has been chosen to be that of the PE. In most experiments, the heating-law characteristic time is of the order of 1 s, which corresponds to the order of magnitude of the PE characteristic time.

The calculations were performed for supercritical CO_2 which is initially 1 K from the critical temperature and comparisons were made with the perfect gas at standard conditions, i.e. $T_0' = 300$ K and $\rho_0' = 1.8$ kg m^{-3}. The boundary conditions for the perfect gas are the same as for a supercritical fluid and the initial conditions can be written as

$$\rho_0 = 1, \quad T_0 = 1, \quad P_0 = 1, \quad u = v = 0.$$

3. Numerical method

3.1. *General description*

The numerical method used in this analysis is based on the finite-volume method with the SIMPLER algorithm which is the Revised-SIMPLE (Semi-Implicit for Pressure Linked Equations) algorithm of Patankar & Spalding (1972). The detailed developments and comparisons of these methods can be found in Patankar & Spalding (1972), Patankar (1980, 1985), Jang, Jetli & Acharya (1986), and Amiroudine *et al.* (1996). The variable 'power-law' type (100×40) mesh follows a geometrical series with a power of 2.5 (see figure 2). Only suitable interpolation will determine values at the variable grid points. The domain is divided into regions and, in each region, one can refine the mesh in both directions. A staggered mesh has been developed where velocity components are defined on the sides of the cell and thermodynamic quantities at the cell centre, to avoid pressure oscillations (Patankar 1980). As we approach the critical point, the boundary layer becomes very thin and one needs a small grid size in order to have a relatively small cell Péclet number. In all our calculations, stability in terms of time step and grid size has been carefully tested.

The numerical code we have used solves two-dimensional unsteady viscous compressible flows in rectangular cavities on variable meshes. It takes into account hypercompressible flows with physical properties which diverge at the critical point, as shown in (3). Our code has been carefully tested against some relevant benchmark cases. The results of such comparisons can be found in Amiroudine (1995). It is important to note here that, besides the fundamental role played by the physical phenomenology of the problem under study, we demonstrate the feasibility of simulating unsteady near-critical hypercompressible flows using the finite-volume method with the algorithms mentioned above.

The numerical modelling of supercritical fluids which has been developed in recent

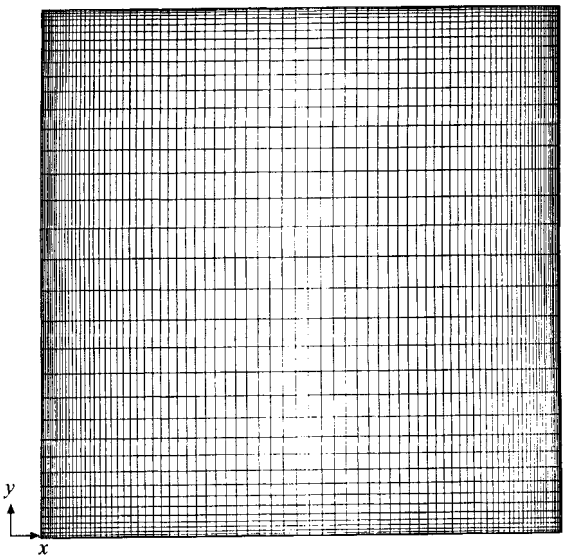

FIGURE 2. The numerical mesh (100×40).

years, mostly for one-dimensional situations (Zappoli *et al.* 1990; Zappoli & Durand-Daubin 1994; Amiroudine *et al.* 1996) and multidimensional numerical studies have not previously been performed for this problem with the method of acoustic filtering described below.

3.2. *Acoustic filtering*

As is the case for normally compressible flows, the acoustic-filtering procedure is necessary to reduce the computational time when an acoustic-wave description is not needed. In fact, without such filtering the semi-implicit character of the present algorithm would not be able to reduce the time step (compared to an explicit one) (Spradley & Churchill 1975) since the time-step reduction is governed mainly by acoustic phenomena and not by stability criteria. On the other hand, as pointed out by Paolucci (1982), for small Mach numbers, implicit schemes making use of relaxation methods are relatively inefficient for time-step reduction and overall pressure changes since the relaxation of long-wavelength errors is a slow process in the low-Mach-number limit.

The thermodynamic field is expanded in terms of the small Mach number (M_a); thus, the pressure is written, e.g.

$$P = P^{(0)} + M_a^2 P^{(1)} + o(M_a^2),$$

and all other variables are expanded in a similar manner. This results in the leading term for pressure being a function of time only and the contribution of the pressure to the momentum equations comes from the $O(M_a^2)$ term.

In practice, in our numerical approach, we have split the pressure as follows:

$$P = \bar{P}(t) + p'(x, y),$$

where the leading term $\bar{P}(t)$ is spatially homogeneous and the perturbation term, which is of order M_a^2, appears only in the momentum equations.

The splitting of the pressure has resulted in one more unknown than the number of

available equations and an extra equation is needed to determine the static pressure $\bar{P}(t)$. This pressure is determined by requiring mass conservation at each time step,

$$\int_{V(t)} \rho \, \mathrm{d}V(t) = \int_{V_0} \rho_0 \, \mathrm{d}V_0,$$

where V represents the volume of the cell and subscript 0 refers to initial values. The method of filtering sound is used for time scales greater than acoustic time scales. Another way to determine this static pressure (Paolucci 1982) is to use the continuity, energy and state equations and integrate $\mathrm{d}\bar{P}/\mathrm{d}t$ over the volume of the cell.

It must be emphasized here that the use of the acoustic-filtering method is consistent with theoretical predictions concerning the evolution of pressure. Indeed, it has recently been shown in a one-dimensional geometry (Zappoli & Carles 1995) that, throughout the evolution of the fluid flow by PE, the pressure could be split into a spatially homogeneous term plus a small acoustic perturbation. The pressure splitting used in the numerical scheme simply reproduces this asymptotic property.

4. Results and discussion

In what follows, the results of the computations just described are analysed with special emphasis on the heat- and mass-transport mechanisms leading to thermal and mechanical equilibrium in the cavity after the temperature of the left-hand sidewall is increased by 10 mK over a period of 1 s. In order to examine the difference between the normal-gas response and that of a supercritical fluid, the same problem has been solved with the same numerical code for CO_2, assuming it behaves as a perfect gas. Although the computations are performed in terms of dimensionless variables, it is more convenient to discuss results in terms of dimensional quantities.

4.1. *Temperature equilibration*

We observe in figure 3(*b*) that at 4.5 s, temperature equilibrium in the cavity is almost achieved through the PE, while the effect of buoyancy is restricted to a low-density thermal plume visible at the hot wall and top-left part of the cavity. This part of the flow field will be described more in detail in §4.3. On the other hand, the perfect gas thermal field shown in figure 3(*a*) for the same time is inhomogeneous because of more rapid thermal diffusion coupled with very weak convection. The density profiles corresponding to these two cases are shown in figure 4. The homogeneous temperature and density fields in the bulk of the cavity for the supercritical fluid at a time much shorter than the thermal-diffusion time are the signature of the PE and show that there is no significant interaction between the buoyant convection and the PE.

In order to analyse the fluid-dynamic mechanisms that occur under normal-gravity conditions, it is helpful to recall what happens under zero-gravity conditions (Zappoli 1992; Zappoli *et al.* 1990; Onuki *et al.* 1990; Boukari *et al.* 1990). The very rapid temperature equilibration in the bulk is due to the strong expansion (decrease in density) of the fluid contained in the thermal boundary layer due to the very large isothermal compressibility of the near-critical fluid. This expansion produces mass addition in the bulk phase and also adiabatic compressive heating. When gravity is set to its ground value, as soon as mass depletion occurs in the thermal boundary layer a buoyant vertical-velocity component appears which does not significantly change the thermal structure of the thermal boundary layer (except in the upper left corner), since this vertical velocity is parallel to the isotherms. The thermal structure of the boundary

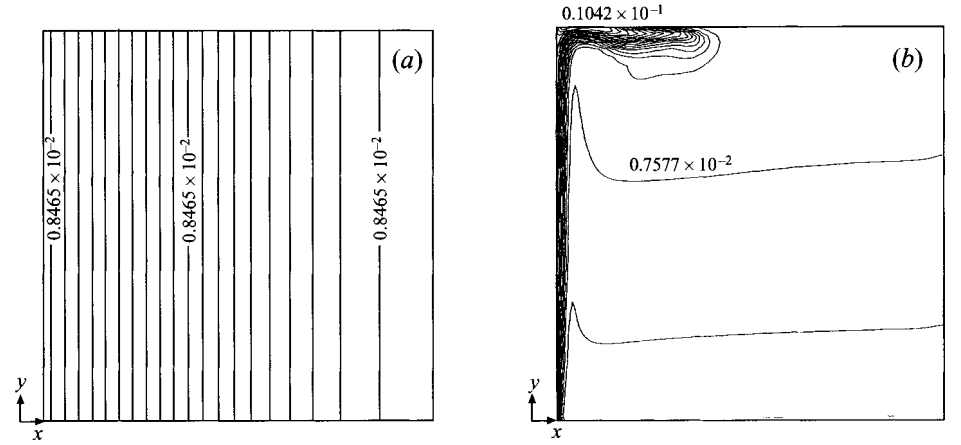

FIGURE 3. Temperature difference field in K for (*a*) the perfect gas and (*b*) the supercritical fluid for 1*g* at 4.5 s.

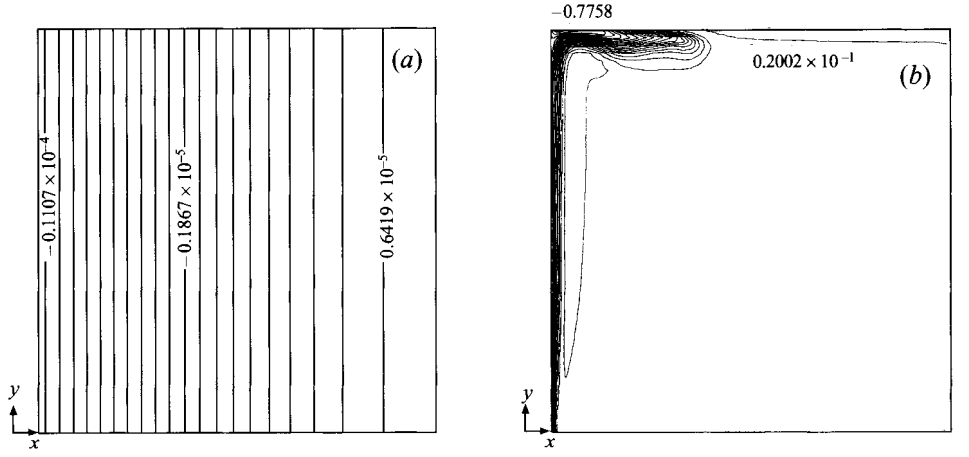

FIGURE 4. Density difference field in kg m^{-3} for (*a*) the perfect gas and (*b*) the supercritical fluid for 1*g* at 4.5 s.

layer and thus the net mass loss out of it, is not significantly changed from the one-dimensional situation (Zappoli 1992; Zappoli & Durand-Daubin 1994; Zappoli *et al.* 1990; Amiroudine *et al.* 1996), although the buoyant vertical velocity is much higher than the horizontal one, as can be seen in figure 5, which shows the velocity at the end of the heating period (at $t = 1$ s). The total mass transferred to the bulk is thus nearly convection-independent and this is the reason why the PE is responsible for temperature equilibration of the bulk even in the presence of convection.

This result seems to be inconsistent with measurements performed by D. Beysens (1995, personal communication), who reports that the efficiency of the PE in homogenizing temperature would be *less* on ground than under microgravity conditions. However, the geometrical configuration considered here is quite different from in Beysens's experiments (heating is provided by a small spherical thermistor immersed within the fluid), and the boundaries are at constant temperature. Therefore, the thermal plume rising from the thermistor may interact with the upper boundary in such a way (i.e. through a PE from the top wall) to reflect back the energy it just

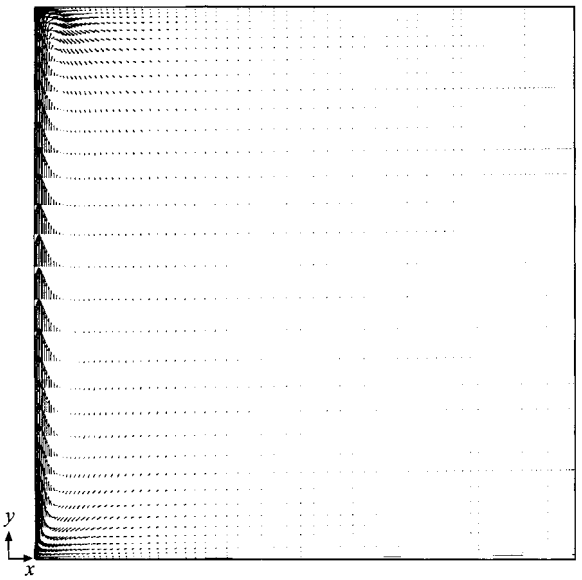

FIGURE 5. Velocity field for the supercritical fluid for 1g at 1 s. The maximum vector plot is 7.2×10^2 μm s^{-1}.

received, and thus to decrease the thermoacoustic coupling. This particular point has to be checked independently but seems consistent with previous theoretical and experimental results concerning the PE in thermostated cells (Zappoli & Carles 1995; Garrabos *et al.* 1996).

The temperature is plotted in Figure 6(*a*) as a function of x at $y = 0.5$ for several times during the temperature equilibration period for both the supercritical fluid and the perfect gas. The supercritical fluid exhibits the characteristic profiles of the PE (a very thin thermal boundary layer followed by a thermally homogeneous bulk) and the perfect gas shows a diffusive profile. For the density field, we observe some very interesting features as seen in figure 6(*b*), which shows profiles for both the supercritical fluid and the perfect gas near the heated wall at $y = 0.5$ for two times belonging to the PE period. The first observation is that the density of the supercritical fluid is four orders of magnitude larger than that for a perfect gas owing to the very high compressibility of the supercritical fluid. The second is that the boundary layer is much thinner for the supercritical fluid than for the perfect gas. The direct consequence of these two features concerning the density field is, of course, the structure of the buoyant convection field.

Figure 7 shows the vertical velocity as a function of x at $y = 0.5$ for the supercritical fluid and the perfect gas at a time of 1 s. The result is a much larger vertical velocity occurring in a much thinner boundary layer for the supercritical fluid than for the perfect gas. Secondly, while the driving force for convection (the density gradients) fills the entire cavity for the perfect gas, thus producing a velocity field of homogeneous magnitude, the driving force for convection in the supercritical fluid is limited to a very thin boundary layer. However, a significant upward velocity extends far beyond this boundary-layer thickness, which shows that the fluid located near the boundary layer is drawn upward by viscous coupling. This is confirmed in figure 8 where velocity vectors are shown for the two cases at a time of 4.7 s. While the perfect gas exhibits a classical circular one-roll pattern, the supercritical fluid exhibits a pattern reminiscent of zero-gravity Marangoni (Carpenter & Homsy 1990) convection (in which the left-

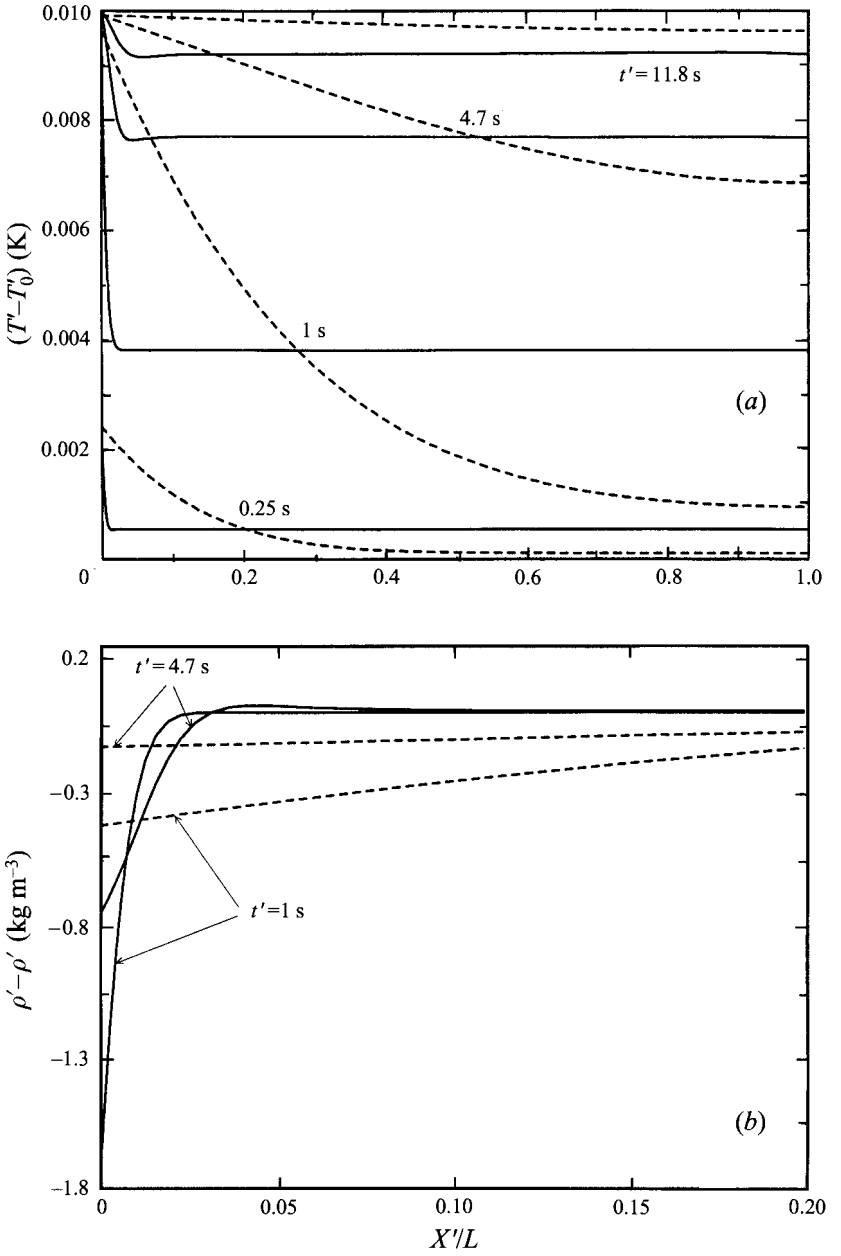

FIGURE 6. (*a*) Temperature difference and (*b*) density difference, for the perfect gas (– – –) (times 10^4 in *b*) and the supercritical fluid (——) as a function of x at different times and at $y = 0.5$.

hand-side heated wall would be replaced by a free surface). It should also be emphasized that the intensity of convection for the supercritical fluid is about 3×10^2 larger for the supercritical fluid than for the perfect gas.

Based on the results presented in figures 7 and 8, we return to the initial question concerning the mode of heat transport in a supercritical fluid under normal gravity conditions, namely: (i) is the PE responsible for fast heat equilibration?; (ii) if yes, as it currently appears to be, is there still convection?; and (iii) if yes, as is the case again, why is this so, since the thermal field is homogeneous? The answers to these questions

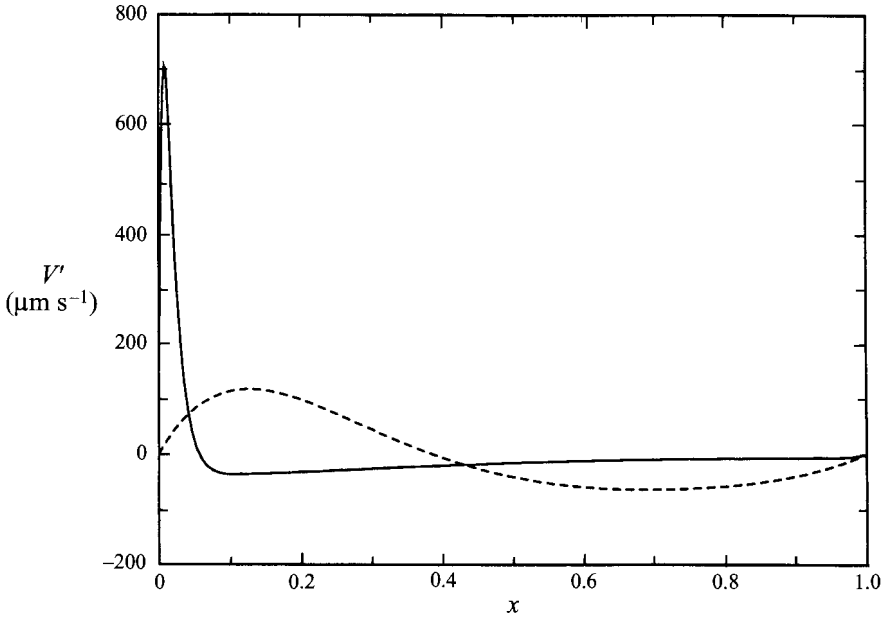

FIGURE 7. Vertical velocity for the supercritical fluid (——) and the perfect gas (– – –) (times 10) as a function of x at 1 s.

are linked to the density-relaxation problem, which is currently being investigated, both theoretically and experimentally, on the ground (Boukari *et al.* 1995; Zhong & Meyer 1995) and under microgravity conditions (Bailly, Ermakov & Zappoli 1996; R. A. Ferrel 1994, personal communication). The present findings concerning mass equilibration are discussed in the following section in the light of the current studies.

4.2. *Density homogenization*

The results of the present computations, which show thermal equilibration occurring on a much shorter time scale than that for density, are in agreement with recent observations by others. Onuki *et al.* (1990) have shown that after boundary heating under microgravity conditions, density equilibration in the bulk should ultimately follow the long exponential diffusive tail of the temperature inhomogeneity. Guenoun *et al.* (1993) have reported that a phase-separating pure fluid which is heated again above its critical temperature exhibits long-lasting density inhomogeneities, although the bulk temperature has risen homogeneously above the critical temperature due to the PE. Boukari *et al.* (1995) have shown by numerical solution of the one-dimensional convectively-stable flow equations that the formation, on the ground, of the density profile following a temperature quenching of the lower boundary, could take hours, whereas temperature is equilibrated very quickly by the PE. Similar observations have been reported in experiments by Zhong & Meyer (1995). Also it has been shown (Bailly *et al.* 1996) that, under microgravity conditions, the density homogenization in the bulk phase following boundary heating occurs in two periods. The first is a fast period, already mentioned by Zappoli (1992), and described by Zappoli & Durand-Daubin (1994) and Onuki & Ferrell (1990), during which density decays from its initial value α/μ (where α is the order of magnitude of the temperature increase at the boundary and μ the initial distance to the critical point) to α. This is followed by a slow period (which is the new finding), driven by the very long thermal-diffusion process (since the thermal diffusivity approaches zero for a supercritical fluid), during which density relaxes from

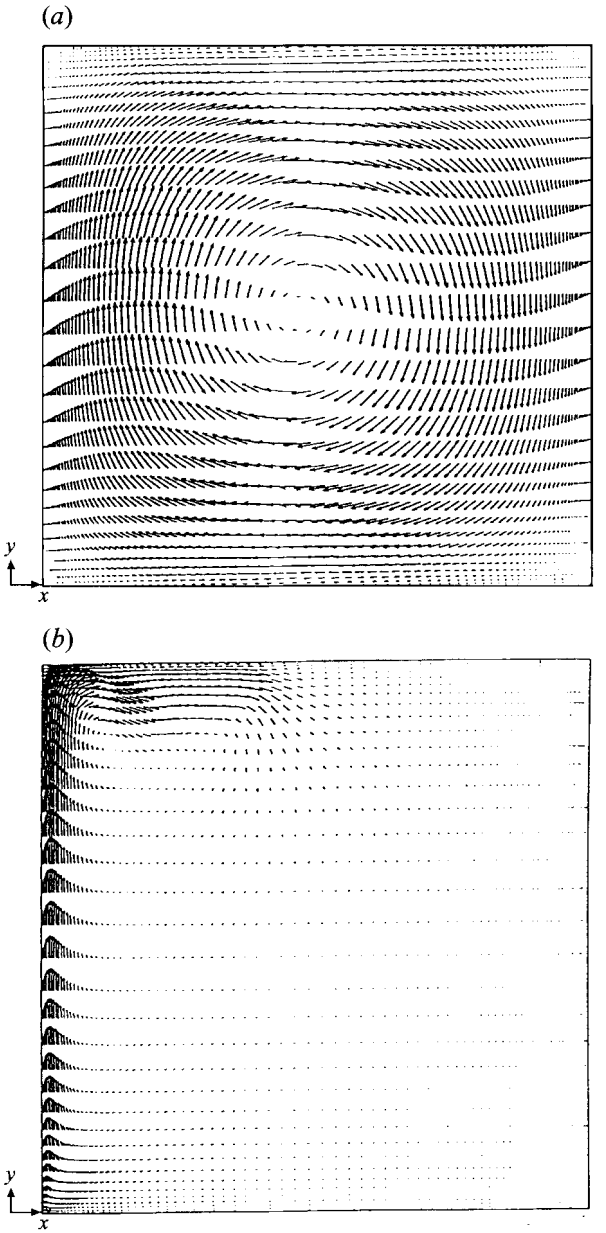

FIGURE 8. Velocity field for (*a*) the supercritical fluid and (*b*) the perfect gas for 1*g* at 4.7 s. The maximum vector plot is 2.2×10^3 μm s^{-1} in (*a*) and 6.5 μm s^{-1} in (*b*).

α to $\alpha\mu$, that is, to equilibration, while the temperature difference, which decreased from α to $\alpha\mu$ during the PE period, decreases further to $\alpha\mu^2$.

The difference between the equilibration times for temperature and density is therefore shown to arise from the large order of magnitude difference between the temperature and density perturbations. The answer to the question regarding the presence of convection after the thermal field is uniform thus follows from the preceding discussion: owing to the very larger compressibility, the remaining temperature inhomogeneity (of order $\alpha\mu$) left by the PE gives rise to a significant density inhomogeneity which relaxes very slowly, together with heat diffusion, leaving

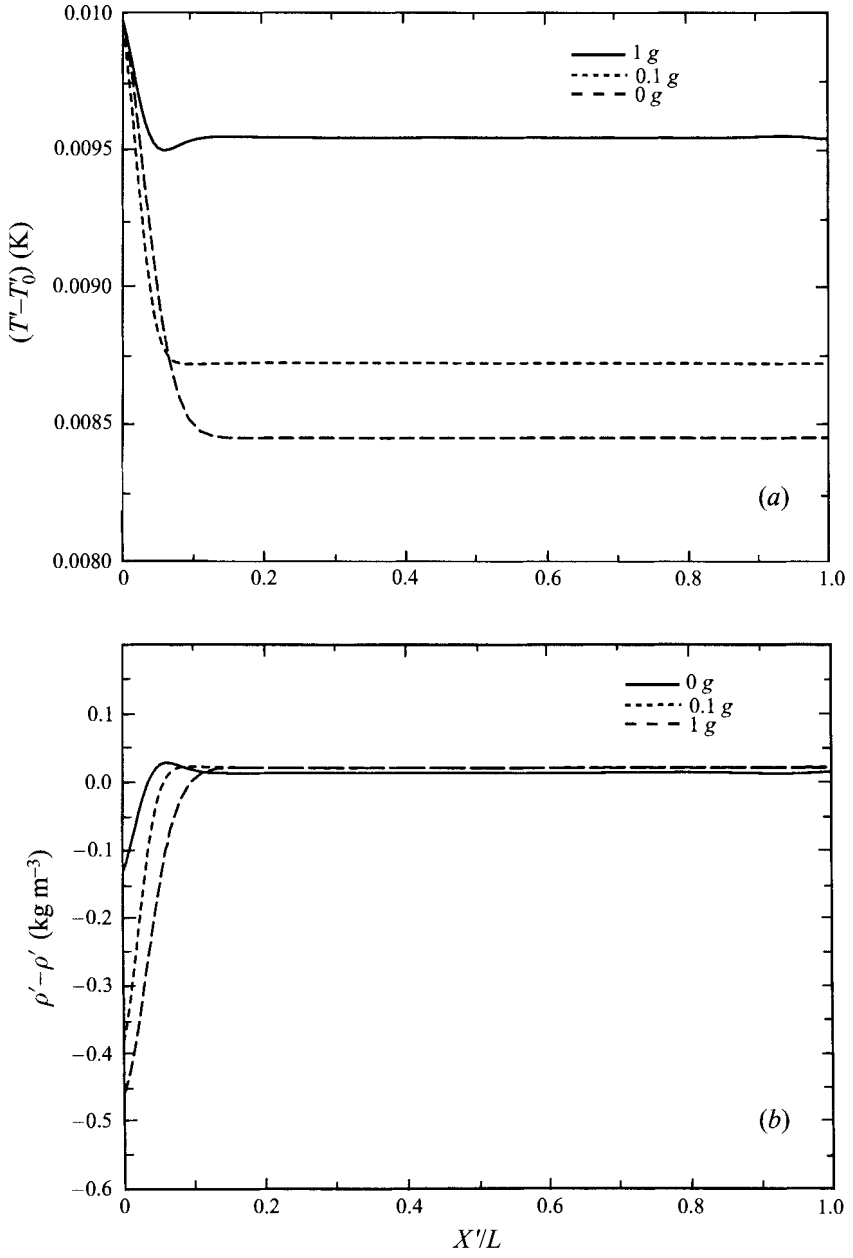

FIGURE 9. (*a*) Temperature difference and (*b*) density difference for the supercritical fluid as a function of x at different levels of gravity at $t' = 16.6$ s.

time for gravity to generate significant convection in a quasi-isothermal medium. We thus observe a convection motion occurring in a quasi-isothermal, pure fluid which could be called 'isothermal critical convection'. On the ground, given the long heat-diffusion time scale, the return flow has time to compensate the mass depletion still existing in the heated region, thus speeding up the mass equilibration process. In microgravity, equilibration of the density field takes even longer since only diffusion occurs. This can be seen in figure 9(*b*), which shows clearly that, under increasing gravity, the mass depletion in the thermal boundary layer is reduced. It must be also

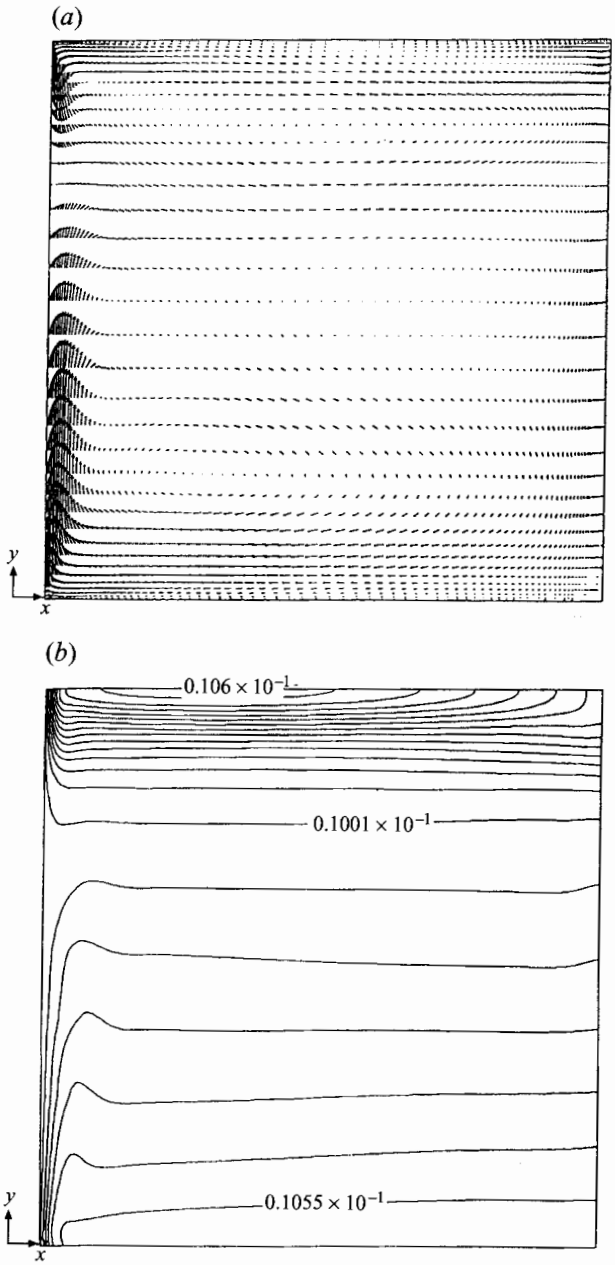

FIGURE 10. (*a*) Velocity field (maximum vector plot is 2.24×10^2 μm s^{-1}), and (*b*) temperature difference field in K, for the supercritical fluid for 1*g* at 35.5 s.

emphasized that, owing to the long density-homogenization time, the convective pattern is quasi-steady on the convective time scale. The role of convection in a near-critical fluid is clearly to homogenize density which would otherwise relax very slowly by pure thermal diffusion alone. Figure 9(*a*), which represents temperature as a function of x at $y = 0.5$ for different gravity levels, confirms that the PE is responsible for 85% of the equilibration in zero gravity; only 10% more is achieved through the addition of convection. Examples of isothermal-critical-convection flow patterns are given in figures 10 and 11, which exhibit an unusual two-roll pattern, the origin of

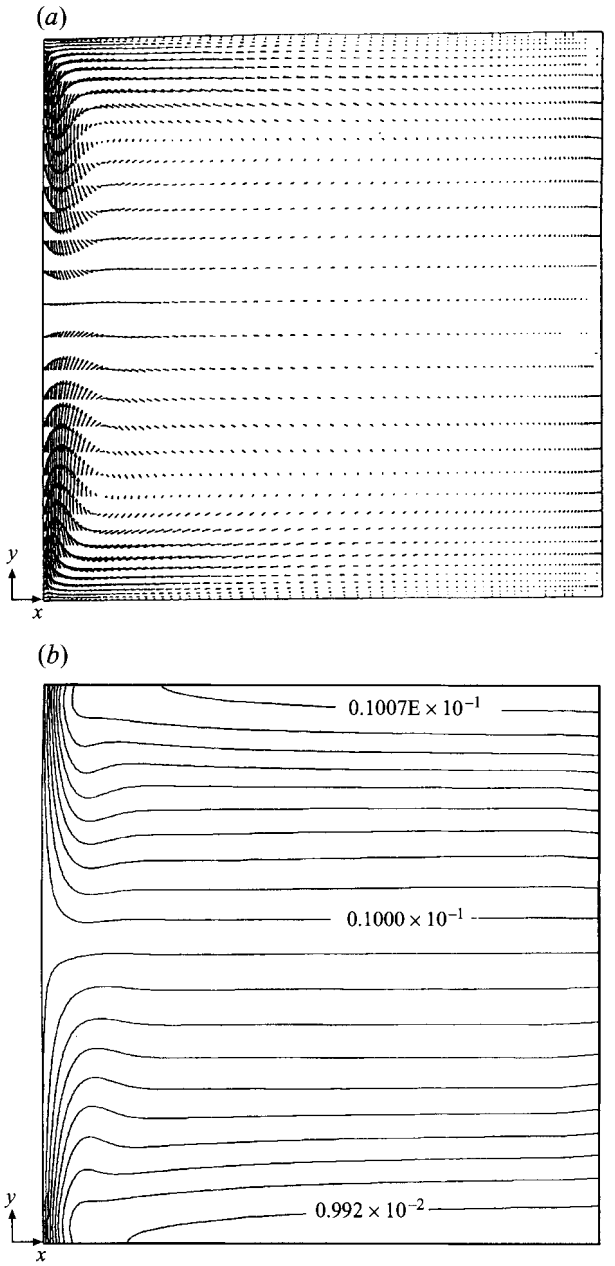

FIGURE 11. As figure 10 but at 713 s (maximum vector plot is 8.6×10 μm s^{-1}).

which will be discussed in the next section. It should be noted that the fluid velocity in the supercritical fluid, more than ten minutes after the heating has been stopped, is still more than ten times its magnitude in the perfect gas only some seconds after the end of the heating period. The convection roll intensity then decreases slowly in time on the diffusion time scale. The calculation has not been continued to a state of uniform density due to the required computational time and the lack of additional insight it would bring to the problem.

4.3. *Stagnation-point effect and the two-roll pattern of isothermal quasi-steady critical convection*

The interaction between the thermal plume and the upper left corner of the cavity that begins to occur within the PE time scale mentioned in §4.1, requires additional discussion. As shown on the temperature plots, this is a very hot region, even hotter than the boundary itself. This is clearly not an artifact of the numerical procedure, since mesh refinement effects in the corresponding region as well the influence of time step on the overheating of the upper wall have been carefully checked. Therefore, the following mechanism is proposed. During the rise of the supercritical fluid particle along the heated wall, the gain in kinetic energy for a very small temperature increase at the boundary is much higher than it would be in a perfect gas, due to the strong density decrease in the thermal boundary layer. On the other hand, the vertical pressure gradient is quite small (because of the low Mach number of the flow; see §3.2), so that the increase in kinetic energy results from the work of the buoyancy force. When the thermal plume reaches the upper, insulated boundary, a turning flow region forms that surrounds a stagnation point where kinetic energy turns into internal energy (thus explaining the hot spot) and into work of pressure forces in expanding the fluid because of the high isothermal compressibility. To deepen the understanding of this effect, it is worth considering what happens in other situations.

In high-speed flows of normally compressible fluids, the transformation of kinetic energy into internal energy comes from the dynamic effects of the fluid that cause pressure gradients according to the velocity-pressure coupling. In low-speed convective flows, the velocity-pressure linkage weakens in the low-Mach-number limit and the pressure-source term in the internal-energy equation is negligible owing to the moderate compressibility. Therefore, temperature is governed by diffusion and convection, density is coupled with temperature and it is thus unusual to find this effect in Boussinesq fluids.

In low-Mach-number hypercompressible flows of a supercritical fluid, the pressure is still homogeneous because of the weak velocity–pressure coupling (as for normal gases), but due to the high thermal expansion coefficient, there is an enhancement of the density–temperature coupling. This leads to a strong velocity–temperature coupling through the velocity-divergence term in the pressure-work forces of the internal-energy balance which is responsible for the overheating of the upper wall. However, the increase in the kinetic energy is not a necessary condition for finding transient temperature overshooting, as for example, reported by Zhong & Meyer (1995) and Boukari *et al.* (1995) for quite different situations. When the top and bottom plates are both heated (Boukari *et al.* 1995), during the rearrangement of the one-dimensional density profile due to stratification, both experiments and one-dimensional calculations lead to a bulk top temperature which overshoots the equilibrium temperature. In such a situation, the kinetic energy remains very small and cannot be responsible (through the transfer to internal energy) for the temperature increase as in the present case. However, if the kinetic energy is negligible, the velocity field is responsible for the mass transfer from the boundary layer to the bulk that causes a homogeneous pressure increase in the bulk. This pressure increase converts its mechanical energy into temperature in an inhomogeneous way, owing to the expansion coefficient which varies with density and thus with height. It is likely that convection phenomena very close to the critical point exhibit new thermal behaviour coming from both the dependence of the thermodynamic coefficients on density and from dynamic effects due to the increase in the kinetic energy.

When the gravity force is smaller and acts for a shorter time, as explored by Bravais, Zappoli & Mignon (1993), the temperature of the upper wall does not exceed that of the heated wall, since the work done by gravity is much smaller. The existence of a spot on the upper wall which is hotter than the heated boundary is quite important since it appears to be responsible for the two-roll structure of the long-lasting quasi-isothermal convection. The hotter fluid at the insulated boundary in the upper left corner expands horizontally, but as it flows toward the cooler heated boundary it becomes heavier and begins to flow downward; this can be seen in figure 10 where a counterclockwise roll is appearing in the upper left corner. Then, as heat is slowly carried away by diffusion, the hot region widens and so does the corresponding roll (figure 11). At the same time, the return flow decreases the density depletion of the thermal boundary later, and thus, the magnitude of the kinetic energy increases there. The hot region thus tends to disappear as time goes by, both by diffusion and by the decrease in the thermomechanical coupling.

5. Conclusions

A two-dimensional unsteady numerical code has been developed which is able to simulate hypercompressible low-Mach-number buoyant-convection flows. This has been applied to a particular problem involving near-critical fluids subjected, under normal gravity conditions, to heat addition at a boundary. The results of these computations have identified some important basic mechanisms of heat transport, mass equilibration and the existence of interesting convective structures. As expected, the description of convective motion in a dense liquid which can be 10^4 times as compressible as a perfect gas has been a numerical challenge. The numerical solution of the Navier–Stokes equations for this case has been successfully achieved using a finite-volume method with the SIMPLER algorithm, together with acoustic filtering which proved to be the most efficient in terms of precision and computational cost.

The results demonstrate that the high compressibility of near-critical fluids and their low heat diffusivity lead to a decoupling of the heat- and mass-equilibration processes. The PE initially homogenizes the temperature on a very short time scale (shown to be convection-independent) compared to diffusion and identical to the microgravity PE time scale. At the end of this PE time period, the thermal field is almost completely homogenized while density differences are still significant owing to their very large initial value. These remaining density inhomogeneities then relax very slowly to equilibrium by (slow) thermal diffusion, providing time for convection to begin. This is similar to what is observed for a normal gas, but convection persists for a very long time in the case of a supercritical fluid in an already thermalized fluid. We have termed this phenomenon *quasi-steady isothermal critical convection* and its structure has been explored so as to emphasize its peculiarities *vis à vis* normal gases under the same heating conditions. Whereas normal gases exhibit a classical single-roll structure, near-critical convection first exhibits a Marangoni-like structure during the fast PE period, then (owing to the presence of the overheating of the upper, insulated boundary due to a surprising stagnation point effect), a long-lasting isothermal convection with an original counter-rotating two-roll pattern. This work clearly points out the important role played by the critical behaviour of the transport coefficients in the formation of convective structures in near-critical fluids, which may have implications for other phenomena such as instability or the onset of turbulence.

The authors gratefully acknowledge support from CNES (Centre National d'Etudes

Spatiales) through IMFM (Institut de Mécanique des Fluides de Marseille), the 'Centre de Calcul de la Région PACA' at IMT (Institut Mediterranéen de Technologie). They also acknowledge Professor G. P. Neitzel for careful reading of the manuscript and fruitful discussions.

REFERENCES

AMIROUDINE, S. 1995 Modélisation numérique des phénomènes de transport de chaleur et de masse dans les fluides supercritiques. PhD dissertation, Institut de Mécanique des Fluides, Marseille, France.

AMIROUDINE, S., OUAZZANI, J., ZAPPOLI, B. & CARLES, P. 1996 Numerical solutions of 1D unsteady hypercompressible flows using finite volume methods. *Eur. J. Mech.* (submitted).

BAILLY, D., ERMAKOV, M. & ZAPPOLI, B. 1996 Density relaxation in near critical pure fluids. *Phys. Rev.* A (to be submitted).

BONETTI, M., PERROT, F., BEYSENS, D. & GARRABOS, Y. 1994 Fast thermalization in supercritical fluids. *Phys. Rev.* E **49**, R4779.

BOUKARI, H., SHAUMEYER, J. N., BRIGGS, M. E. & GAMMON, R. W. 1990 Critical speeding up in pure fluids. *Phys. Rev.* A **41**, 2260.

BOUKARI, H., PEGO, R. L. & GAMMON, R. W. 1995 Calculation of the dynamics of gravity-induced density profiles near the liquid-vapor critical point. *Phys. Rev.* E **52**, 1614.

BRAVAIS, P., ZAPPOLI, B. & MIGNON, C. 1993 Free convection in the vicinity of the critical point. *Presented at the 14th IAF Congress, Gratz, Austria. Acta Astronautica* (to appear).

CARLES, P. 1995 L'Effet piston et les phénomènes thermoacoustiques dan les fluids supercritiques. PhD dissertation, Institut National Polytechnique de Toulouse, France.

CARPENTER, B. M. & HOMSY, G. M. 1990 High Marangoni number convection in a square cavity: Part 2. *Phys. Fluids* A **2**, 137.

GARRABOS, Y., BONNETTI, M., BEYSENS, D., PERROT, F., FROHLICH, T., CARLES, P. & ZAPPOLI, B. *Phys. Rev.*, (in preparation).

GITTERMAN, M. & STEINBERG, V. A. 1970 Criteria of occurrence of free convection in a compressible viscous heat-conducting fluid. *J. Appl. Math. Mech.* **34**, 305.

GITTERMAN, M. & STEINBERG, V. A. 1972 Establishment of thermal equilibrium in a liquid near the critical point. *High Temp.* **10**, 565.

GUENOUN, P., BEYSENS, D., KHALIL, B., GARRABOS, Y., KAMMOUN, B., LE NEINDRE, B. & ZAPPOLI, B. 1993 A thermo cycle around the critical point of CO_2 under reduced gravity. *Phys. Rev.* E **47**, 1531.

HEINMILLER, P. J. 1970 A numerical solution of the Navier–Stokes equations for supercritical fluid thermodynamic analysis. *T.R.W. Rep.* 17618-H080-RO-00. Houston, Texas.

JANG, D. S., JETLI, R. & ACHARYA, S. 1986 Comparisons of the PISO, SIMPLER and SIMPLEC algorithms for the treatment of the pressure-velocity coupling in steady flow problems. *Number. Heat Transfer* **10**, 209.

KLEIN, H., WANDERS, K. & FEUERBACHER, B. 1991 Relaxation of non-equilibrium density inhomogeneities in near critical fluids. *Adv. Space Res.* **11**, 181.

MOLDOVER, M. R., SENGERS, J. V., GAMMON, R. W. & HOCKEN, R. J. 1979 *Rev. Mod. Phys.* **51**, 79.

ONUKI, A. & FERRELL, R. A. 1990 *Phys. Rev.* A **164**, 245.

ONUKI, A., HAO, H. & FERRELL, R. A. 1990 Fast adiabatic equilibrium in a single component fluid near the liquid-vapor critical point. *Phys. Rev.* A **41**, 2256.

PAOLUCCI, S. 1982 On the filtering of sound from the Navier–Stokes equations. *SAND* 82-8257.

PATANKAR, S. V. 1980 *Numerical Heat Transfer and Fluid Flow.* Hemisphere.

PATANKAR, S. V. 1985 A calculation procedure for two-dimensional elliptic situations. *Number. Heat Transfer* **14**, 409.

PATANKAR, S. V. & SPALDING, D. P. 1972 A calculation procedure for heat, mass and momentum transfer in three dimensional parabolic flows. *Intl J. Heat Mass Transfer* **15**, 1787.

SPRADLEY, L. W. & CHURCHILL, S. W. 1975 Pressure and buoyancy-driven thermal convection in a rectangular enclosure. *J. Fluid Mech.* **70**, 705.

STANLEY, H. E. 1971 *Introduction to Phase Transition and Critical Phenomena.* Clarendon.

STRAUB, J. 1965 Dissertation, Technische Universitt, Munchen, Germany (unpublished). Results presented by E. H. Schmidt in *Critical Phenomena* (ed. M. S. Green & J. V. Sengers), *Proc. Conf. on Phenomena in the Neighbourhood of Critical Point (National Bureau of Standard, Washington, DC*, 1966).

STRAUB, J. & NITSCHE, K. 1991 In *Proc. 11th Symp.* on *Thermophysica Properties, Boulder, Colorado.*

STRAUB, J. & NITSCHE, K. 1993 Isochric heat capacity C_v at the critical point of SF_6 under micro and earth-gravity. Results of the German spacelab mission D_1. *Fluid Phase Equil.* **88**, 183.

SWINNEY, H. L. & HENRY, D. L. 1973 Dynamics of fluids near the critical point: decay rate of order-parameter fluctuations. *Phys. Rev.* A **8**, 2586.

ZAPPOLI, B. 1992 The response of a nearly supercritical pure fluid to a thermal disturbance. *Phys. Fluids* A **4**, 1040.

ZAPPOLI, B., BAILLY, D., GARRABOS, Y., LE NEINDRE, B., GUENOUN, P. & BEYSENS, D. 1990 Anomalous heat transport by the piston-effect in supercritical fluids under zero gravity. *Phys. Rev.* A **41**, 2224.

ZAPPOLI, B. & CARLES, P. 1995 Thermoacoustic nature of the critical speeding-up. *Eur. J. Mech.* B **14**, 41.

ZAPPOLI, B. & CARLES, P. 1996 Acoustic saturation of the critical speeding up. *Physica* D **89**, 381–394.

ZAPPOLI, B. & DURAND-DAUBIN, A. 1994 Direct numerical modelling of heat and mass transport in a nearly supercritical fluid. *Phys. Fluids* **6**, 1929.

ZHONG, F. & MEYER, H. 1995 Density equilibration near the liquid-vapor critical point of a pure fluid: single phase $T > T_c$. *Phys. Rev.* E **51**, 3223.